Structural and Dynamic Perturbations Induced by Heme Binding in Cytochrome b_5[†,‡]

Christopher J. Falzone, Yuemei Wang, B. Christie Vu, Nancy L. Scott, Shibani Bhattacharya, and Juliette T. J. Lecomte*

Department of Chemistry and Center for Biomolecular Structure and Function, The Pennsylvania State University, University Park, Pennsylvania 16802

Received November 22, 2000

ABSTRACT: The water-soluble domain of rat hepatic cytochrome b_5 undergoes marked structural changes upon heme removal. The solution structure of apocytochrome b_5 shows that the protein is partially folded in the absence of the heme group, exhibiting a stable module and a disordered heme-binding loop. The quality of the apoprotein structure in solution was improved with the use of heteronuclear NMR data. Backbone amide hydrogen exchange was studied to characterize cooperative units in the protein. It was found that this criterion distinguished the folded module from the heme-binding loop in the apoprotein, in contrast to the holoprotein. The osmolyte trimethylamine *N*-oxide (TMAO) did not affect the structure of the apoprotein in the disordered region. TMAO imparted a small stabilization consistent with an unfolded state effect correlating with the extent of buried surface area in the folded region of the native apoprotein. The failure of the osmolyte to cause large conformational shifts in the disordered loop supported the view that the specificity of the local sequence for the holoprotein fold was best developed with the stabilization of the native state through heme binding. To dissect the role of the heme prosthetic group in forcing the disordered region into the holoprotein conformation, the axial histidine belonging to the flexible loop (His63) was replaced with an alanine, and the structural properties of the protein with carbon-monoxide-ligated reduced iron were studied. The His63Ala substitution resulted in a protein with lower heme affinity but nevertheless capable of complete refolding. This indicated that the coordination bond was not necessary to establish the structural features of the holoprotein. In addition, the weak binding of the heme in this protein resulted in conformational shifts at a location distant from the binding site. The data suggested an uneven distribution of cooperative elements in the structure of the cytochrome.

Several small *b* hemoproteins, such as cytochrome b_5, myoglobin, and cytochrome b_{562}, present a common pattern of heme binding by which certain secondary structure elements located at the heme cavity adopt a unique and stable fold only under the influence of the prosthetic group (*1*−*3*, and references therein). Similar local refolding coupled to a binding event is observed in many other proteins and functional contexts (*4*) and draws attention to two features of protein architecture. First, the sequence of the regions to be refolded encodes simultaneously instability in the absence of the ligand and a specific three-dimensional structure in its presence. This distinction between fold stability and specificity (*5*) provides a mechanism for adjusting the energetics of ligand binding through the cost of partial refolding. Second, the ability to achieve different levels of polypeptide chain organization with and without ligand demonstrates an irregular distribution of cooperative interactions within the structure. Varying degrees of cooperativity within a native protein are also manifested in nonuniform binding perturbations as seen in H-exchange studies (*6*, *7*) and internal motion studies (*8*, *9*).

The uneven coupling of structural elements with each other suggests that defined pathways exist for the transmission of conformational messages away from the binding site. A statistical thermodynamic analysis aimed at elucidating the molecular origin of cooperativity in several proteins (*10*) indeed proposes that regions of low stability in binding sites play critical roles in relaying binding status to remote locations via a subset of residues. In the study presented here, cytochrome b_5 served as an experimental test case for the importance of low-stability regions in relation to conformational shifts triggered by cofactor binding.

The water-soluble domain of hepatic cytochrome b_5 (cyt b_5)[1] is a redox protein containing a single heme prosthetic group ligated by two axial histidines in both the ferric and ferrous forms. As shown in Figure 1, the heme group is located within a predominantly α-helical pocket (*11*); this cavity is lined with hydrophobic residues that make tight contact with the porphyrin plane. The apoprotein (apocyt b_5) is readily prepared by acid and organic extraction of the *b* heme (*12*). The low-resolution NMR structure of apocyt b_5

[†] This work was supported by National Institutes of Health Grant GM-54217.

[‡] The coordinates have been deposited at the Protein Data Bank as entries 1I87 and 1I8C.

* To whom correspondence should be addressed: Department of Chemistry, The Pennsylvania State University, 152 Davey Laboratory, University Park, PA 16802. Telephone: (814) 863-1153. Fax: (814) 863-8403. E-mail: jtl1@psu.edu.

10.1021/bi002681g CCC: $20.00
Published on Web 03/22/2001

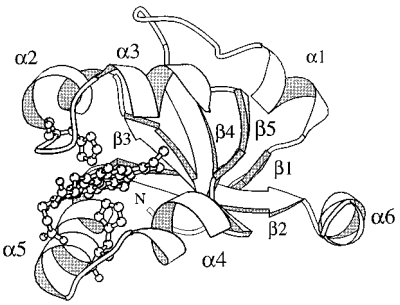

FIGURE 1: Ribbon diagram of the water-soluble domain of cyt b_5 after the X-ray structure of the bovine protein (PDB entry 1cyo). Secondary structure elements are, sequentially, β1, α1, β4, β3, α2, α3, β5, α4, α5, β2, and α6. The heme and the axial histidines are shown with balls and sticks. His39 is located at the end of α2, and His63 is in the extended region connecting α4 and α5. N indicates the N-terminus.

shows a folded structural module formed by an irregular β-barrel and a largely disordered, 30-residue loop in place of the folded heme-binding site depicted in Figure 1 (*1*). The apoprotein exhibits decreased thermal stability compared to the holoprotein (*13*−*15*). However, the unfolding transitions of both the holoprotein and the apoprotein native states are cooperative and can be represented satisfactorily with a two-state model.

The backbone dynamics deduced from ^{15}N relaxation measurements confirm a gain in flexibility in the entire apoprotein (*15*) when compared to the holoprotein (*16*−*18*). In addition, the two axial histidines are not dynamically equivalent in the apoprotein, His39 belonging to the well-folded region of the structure and His63 to the disordered loop. Of particular interest to this work is a third region comprised of helix α6. This helix is located as far from the heme-binding site as the structure allows (Figure 1) and undergoes a conformational equilibrium on the millisecond time scale. Binding the heme group in its cavity suppresses the conformational exchange in helix α6 (*19*).

The goals of this study were to investigate the interactions essential to the establishment of a cooperative network encompassing the heme-binding loop of the cytochrome and helix α6 and to clarify the role of His63 in the coupled binding−refolding event of the apoprotein. These goals required several experimental approaches for refinement of the structural and dynamic description of the loop in the native apoprotein state, inspection of the propensity of the loop to refold in the absence of the heme group, and description of the consequences of severing the coordination bond to His63.

[1] Abbreviations: 1D, one-dimensional; 2D, two-dimensional; 3D, three-dimensional; 2QF, double-quantum filter; apocyt b_5, apoprotein of the water-soluble fragment of rat hepatic cytochrome b_5; ASA, solvent-accessible surface area; cyt b_5, heme-containing, water-soluble fragment of rat hepatic cytochrome b_5; CD, circular dichroism; COSY, correlated spectroscopy; EDTA, ethylenediaminetetraacetic acid; FID, free induction decay; HSQC, heteronuclear single-quantum coherence; NMR, nuclear magnetic resonance; NOE, nuclear Overhauser effect; NOESY, NOE spectroscopy; PAGE, polyacrylamide gel electrophoresis; PDB, Protein Data Bank; ROESY, rotating frame nuclear Overhauser spectroscopy; SDS, sodium dodecyl sulfate; SF, saturation transfer factor; TMAO, trimethylamine *N*-oxide; TOCSY, total correlation spectroscopy; TPPI, time-proportional phase incrementation; Tris, tris(hydroxymethyl)aminomethane; rmsd, root-mean-square deviation; WATERGATE, water suppression by gradient-tailored excitation.

Apocytochrome b_5 was uniformly labeled with ^{13}C and ^{15}N for triple-resonance NMR experiments. Additional NMR restraints were obtained from these spectra, and the low-resolution structure was improved. Backbone amide hydrogen-exchange data were used as complementary markers of local stability and as a means of accessing a dynamic regime slower than characterized by ^{15}N relaxation methods. In favorable cases, H-exchange data can be interpreted in thermodynamic terms to generate a detailed view of cooperative nuclei in proteins (*20*). Although by nature apocyt b_5 did not lend itself to this type of analysis, the exchange behavior provided a criterion for classifying residues according to their conformational lability.

To test further the propensity of the heme loop for adopting regular secondary structure, the conformational properties of apocyt b_5 were inspected anew in the presence of the osmolyte trimethylamine *N*-oxide (TMAO). TMAO has been shown to bring partially folded proteins to their native conformation (*21*, *22*) by generating unfavorable interactions between the backbone and the mixed solvent (*23*). TMAO therefore offered an opportunity to compare unfolded state destabilization with native state stabilization caused by heme binding. Its effect provided a measure of the tendency of the loop to form a compact structure.

Finally, to assess the role of various heme−protein interactions in refolding and to probe a possible pathway of conformational rearrangement within the structure, the axial histidine belonging to the flexible binding loop (His63) was replaced with an alanine. This substitution prevented endogenous hexacoordination of the heme and, by lowering the free energy of heme binding, revealed the contribution of the ligation bond to site 63 in positioning the heme in its cavity.

MATERIALS AND METHODS

Chemicals were purchased from Sigma (St. Louis, MO) unless otherwise indicated. All experiments were conducted in degassed buffers. A 5 M stock solution of TMAO (~99% pure) was treated with activated charcoal or mixed bed ion-exchange resin (Bio-Rad, Hercules, CA) to remove residual amines. The amine-free stock solution was diluted with phosphate buffer (20−60 mM) to a suitable concentration, and the pH was adjusted to the required value. The reported concentrations of TMAO in solution are based on refractive index measurements (*23*).

Cytochrome b_5 Preparation. Unlabeled, ^{15}N-labeled, and ^{15}N- and ^{13}C-labeled wild-type rat hepatic cyt b_5 (water-soluble fragment only) were prepared as previously described (*1*). H63A cyt b_5 was generated with the Quick Change Site-Directed Mutagenesis Kit (Stratagene, La Jolla, CA) by introducing a single base pair substitution to the His63 codon of the wild-type gene in a pET-3d (Novagen, Madison, WI) expression vector. The kit method was modified by transforming the mutated plasmid into competent *Escherichia coli* DH5α cells. The plasmid was purified from overnight cultures using the QIAprep Spin Miniprep Kit (Qiagen, Valencia, CA). The mutant cyt b_5 was expressed in *E. coli* BL21(DE3) cells by following a procedure similar to that used for wild-type cyt b_5 (*1*).

The purification of H63A cyt b_5 was carried out with minor modification of the wild-type protocol. The thawed cells were

resuspended in ion-exchange buffer (IEB) [50 mM Tris, 1 mM EDTA, and 100 mM imidazole (pH 7.5)] and lysed by sonication with six 10 s bursts at 70% power (Fisher Scientific model 60 sonic dismembrator). Cellular debris were separated by centrifugation, and a concentrated solution of bovine hemin chloride in 0.1 M NaOH was added stepwise to the supernatant. After the pH had been lowered to 6 and centrifugation at 48000*g* for 45 min to remove excess hemin, the clarified sample was loaded onto an IEB-equilibrated DEAE Sephacel (Amersham-Pharmacia Biotech, Inc., Piscataway, NJ) anion-exchange column. Elution was performed with a linear salt gradient (from 0.0 to 0.4 M NaCl in IEB). Imidazole was included in the IEB and elution buffer to help preserve the holoprotein form (*24*). Fractions were analyzed by SDS−PAGE, and those essentially free of contaminating proteins were pooled and concentrated to a volume of ∼10 mL. After another hematin reconstitution cycle to compensate for partial hemin loss during anion-exchange chromatography, the remaining contaminants were removed by filtration through Sephadex G-50 fine resin (Amersham) equilibrated with 50 mM Tris and 1 mM EDTA (pH 7.5). Fractions that exhibited a single H63A cyt b_5 band by SDS−PAGE were pooled and concentrated to yield a mixed stock solution of holo- and apoprotein. Pure apoprotein was obtained from this solution by anion-exchange chromatography (as above) in the absence of imidazole. Pure holoprotein was generated by titrating the stock solution with hematin in 0.1 M NaOH. The ferric cyanide complex was produced by addition of excess KCN, whereas the carbonmonoxy complex was prepared by degassing the solution, reducing with solid dithionite, and bubbling CO through the solution for a few minutes. The extinction coefficient of H63A apocyt b_5 at 280 nm was taken to be equal to that of the wild-type protein [10.6 mM^{-1} cm^{-1} in 20 mM phosphate buffer (pH 6.8)].

Far-UV Circular Dichroism Measurements. The CD spectra of wild-type apocyt b_5 and H63A apocyt b_5 were collected between 190 and 290 nm on an Aviv model 62 DS circular dichroism spectropolarimeter. The protein concentration was 0.025 mM in 20−60 mM phosphate buffer (pH 6.8 and 7.3), and the samples were maintained at 25 °C. Wild-type data were also collected in the presence of 0.9 M TMAO. Raw data were corrected by subtracting values collected for buffer over the same wavelength interval and converted into molar residual ellipticity (MRE) (*25*).

Thermal Denaturation. Wild-type apoprotein samples (<0.05 mM) were prepared in 20−60 mM phosphate buffer containing three different concentrations of TMAO (0.25 M at pH 6.5, 0.9 M at pH 6.8 and 7.3, and 1.5 M at pH 6.7). Samples without TMAO were prepared under identical conditions at pH 6.8 and 7.3. H63A apocyt b_5 data were collected at pH 6.7 in the absence of TMAO. Thermal denaturation curves were obtained using an AVIV model 14DS spectrophotometer equipped with a thermoelectric device for temperature control. The absorbance of the apoprotein at 285 nm was monitored by scanning the wavelength between 260 and 320 nm every 0.5 nm. The temperature was varied from 5 to 77 °C in 2 °C increments with 5 min equilibration intervals. This procedure was used in the first trials to verify the presence of isosbestic points. In subsequent trials, data were collected at 285 nm without scanning; the equilibration time was 5 min. The reversibility of the unfolding reaction was tested by returning the samples to the initial temperature and collecting data at 5 °C steps. Reversibility was 95−100% for all apoprotein samples. The absorbance versus temperature data were fitted to a two-state model of denaturation as described elsewhere (*14*, *25*). The equation includes a linear dependence of the extinction coefficient of the fully folded and fully unfolded protein on temperature (requiring four adjustable parameters), the standard enthalpy change ($\Delta H°$), the temperature at the midpoint of the transition (T_m), and a temperature-independent standard change in heat capacity ($\Delta C_p°$). This last parameter is not accurately determined by the method (*14*). The thermal unfolding of the holoprotein carried out under the same conditions that were used for the apoprotein was not reversible in any of the TMAO concentrations.

NMR Spectroscopy. The wild-type cyt b_5 samples were prepared from lyophilized protein, whereas the H63A cyt b_5 samples were obtained by concentrating the solution resulting from the last purification step. Typically, the samples were at concentrations of 1−2 mM in ^1H_2O; the pH was adjusted to the desired value using ^2HCl or NaO^2H, and further ^2H_2O was added to reach a final ^2H_2O concentration of 5−10% of the total sample volume. The ^1H spectra were referenced to the water resonance at 4.76 ppm; ^{13}C signals and ^{15}N signals were referenced indirectly to the proton frequency (*26*). H63A cyt b_5 was subjected only to homonuclear 1D and 2D experiments.

NMR data were acquired on a Bruker AMX2-500 spectrometer (11.7 T, operating at a ^1H frequency of 500.13 MHz) and a Bruker DRX-600 spectrometer (14.1 T, operating at a ^1H frequency of 600.13 MHz). Homonuclear experiments (2QF-COSY, TOCSY, and NOESY) were carried out as reported elsewhere (*1*, *27*). $^1H-^{15}N$ 3D NOESY-HSQC and $^1H-^{15}N$ 3D TOCSY-HSQC data were collected at 14.1 T to confirm the spectral assignments of the wild-type apoprotein in the presence of TMAO. Parameters were as described previously (*15*).

Triple-resonance 3D experiments at 14.1 T were performed on a ^{13}C- and ^{15}N-labeled wild-type apoprotein sample in a 95% H_2O/5% ^2H_2O mixture to complete the spectral assignments and derive additional distance restraints. Parameters are given for dimensions t_1-t_3 with asterisks indicating the number of complex data points: $^1H-^{13}C$ HCCH-TOCSY and COSY (^1H, 4808 Hz and 64*; ^{13}C, 11 468 Hz and 40*; ^1H, 4808 Hz and 512*) (*28*), $^1H-^{13}C$ HSQC-NOESY (^1H, 8013 Hz and 64*; ^{13}C, 11 468 Hz and 32*; ^1H, 8013 Hz and 512*) (*29*), HNCA (^{15}N, 2222 Hz and 44*; ^{13}C, 5000 Hz and 48*; ^1H, 8013 Hz and 512*) (*30*, *31*), and CBCA(CO)NH (^{13}C, 8929 Hz and 60*; ^{15}N, 2222 Hz and 24*; ^1H, 8013 Hz and 512*) (*32*). In all these experiments, quadrature detection in the indirect dimensions was achieved using the TPPI−States method (*33*) and a WATERGATE solvent suppression scheme was used (*34*, *35*).

Data sets were processed using FELIX 97.0 (Molecular Simulations Inc., San Diego, CA). In general, the FID along the direct dimension was convoluted with a low-order polynomial to remove the residual water signal before filtering with a sine-squared window function phase-shifted by 40−60°. Along the indirect dimensions, the interferograms were extended by linear prediction before apodizing with a sine-squared window function phase-shifted by 60−90°. Final data set sizes were typically 512−1024 × 64−128 × 128 real data points. Wild-type apoprotein chemical shifts

are provided as Supporting Information (Tables S1 and S2).

To monitor the effect of 1 M TMAO on the backbone dynamics of the wild-type apoprotein, $^1H-^{15}N$ NOE experiments (*36*) were carried out at 14.1 T with 3 s saturation of the amide protons using a WALTZ-16 decoupling scheme (*37*); the TMAO signal was suppressed with a low-power proton pulse during an additional 1.2 s relaxation delay. The reference spectrum was identical in all respects except for the saturation of the amide protons. The standard deviation on the NOE measurement was typically 8% as reported previously in the absence of TMAO (*15*).

For the hydrogen exchange experiments, ^{15}N apocyt b_5 was dissolved in 20 mM phosphate buffer containing 0.9 M TMAO at pH 7.3 to obtain a final protein concentration of ~1 mM. An identical sample was prepared without TMAO. A second pair of samples was made at pH 6.7 (45 mM phosphate and 0.9 M TMAO).

Saturation transfer methods were applied to measure k_{ex}, the apparent rate constant for the exchange process. In the chosen implementation of the experiment, two $^1H-^{15}N$ HSQC spectra are collected, one without perturbation of the water line, yielding cross-peak intensity I_o, and the other with complete saturation of the water, yielding cross-peak intensity I (*38*). The saturation factor, SF, measures the relative decrease of intensity and is given by

$$\frac{I}{I_o} = \frac{\rho}{\rho + k_{ex}} \qquad (1)$$

where ρ is the selective longitudinal relaxation time of the proton under analysis (*39*). The relaxation delay was set to 2 s, and the water was saturated for 1 s at low power (~50−100 μW). Other parameters for the HSQC collection were as reported previously (*15*).

For practical reasons, it is customary to use a single nonselective T_1 instead of the ρ parameter (*40*). Nonselective ^1H T_1's were measured in the absence of water saturation using an inversion recovery scheme (*38*). The recovery times ranged from 2 to 100 ms. Peak intensities were fit as a function of mixing time (t) according to

$$I(t) = I_o\left\{1 - (1 - \cos\varphi)\exp\left[-\frac{t}{T_1(\text{app})}\right]\right\} \qquad (2)$$

where I_o is the fully relaxed intensity, φ represents the variable flip angle, and T_1(app) is defined as $T_1 + 1/k_{ex}$. Combining eqs 1 and 2 yields estimates of T_1 and k_{ex}. Experimental errors were too large to give significance to individual k_{ex} values, and protection factors (k_{ex}/k_{rc}) were not determined.

The intrinsic exchange rates (k_{rc}) at a given pH and temperature were calculated using standard parameters (*41*). To verify that these values could be used in the presence of TMAO as well, a series of exchange experiments were performed on a model undecapeptide representing a histidine-containing fragment of the G helix of sperm whale myoglobin (IIHVLHSRHPG). This peptide was purchased from the Peptide Synthesis Facility of Washington University (St. Louis, MO). The samples contained 4 mM peptide in 20 mM phosphate buffer with, or without, 0.9 M TMAO at pH 6.8. The sample without TMAO was used to obtain the amide proton chemical assignments with 2QF-COSY and TOCSY data. NOESY data showed no evidence of residual structure in solution at room temperature. Exchange rates were determined by inversion recovery with and without saturation of the water during the mixing time (*40*). Individual T_1(app) values obtained through eq 2 were used as $1/\rho$ in eq 1 to extract values for k_{ex}. Complete saturation of the water was accomplished with a low-power 3 s pulse. In addition, data were collected with a 1D version of the WEX filter (*42*). The mixing times ranged from 1 ms to 1 s. The WEX method requires knowledge of the water longitudinal relaxation rate. This parameter was measured by inversion recovery with application of a weak gradient pulse during inversion and recovery to prevent radiation damping. The values were 3.2 and 2.5 s in 0 and 1 M osmolyte, respectively, an indication of increased bulk viscosity with the osmolyte. The exchange rates obtained by the WEX method and the saturation transfer method, though not identical to the calculated k_{ex}, were within experimental error of each other in the presence and absence of TMAO.

Details of the data processing for obtaining exchange rates from the saturation transfer experiments (*38*) and the WEX experiments (*42*−*44*) are provided in the original references. Because the methods could not be used in a quantitative manner with apocyt b_5, they are not discussed further.

pH Titration. A pH titration of H63A apocyt b_5 was performed by using two identical samples (1 mM) beginning at pH ~7.5. The samples were titrated with 1−4 μL aliquots of either 0.1 M ^2HCl until the pH reached 5.4 or 0.1 M NaO^2H until the pH reached 9.8. The pH was measured before and after each NMR spectrum was acquired; the average values were used for data fitting. The resulting chemical shift versus pH curves for the CϵH of each His residue were fitted by a nonlinear least-squares routine using a modified Henderson−Hasselbach equation:

$$\delta_o = \delta_{His} + (\delta_{His^+} - \delta_{His})\frac{10^{n(pK_a - pH)}}{1 + 10^{n(pK_a - pH)}} \qquad (3)$$

where δ_o is the observed shift at any pH, δ_{His} represents the chemical shift of the neutral form (high pH limit), δ_{His^+} is the chemical shift of the protonated form (low pH limit), and n is a Hill coefficient. The routine converges on the optimal set of pK_a, δ_{His}, δ_{His^+}, and n. The apparent pK_as so determined were compared with the known wild-type values (*45*).

Ring Current Shift Calculations. Ring current shifts caused by the heme group and aromatic residues were calculated with a Johnson−Bovey algorithm (*46*) as described previously (*47*). The values reported in Table 5 are from an eight-loop procedure for the heme group.

Structure Calculations. Structures were calculated using the program X-PLOR 3.851 (*48*) with the protocol based on a hybrid distance geometry-simulated annealing (DG-SA) method. A total of 997 restraints were applied as described in detail in the Results and Table 1. The same approach was applied as previously reported for the medium-resolution structure (*1*) except that the energy maintaining the planarity of the peptide bond was lowered to provide better sampling about this bond. The structures presented have a more realistic range of ω angles, but they also have a larger rmsd than structures with a stiff peptide bond. A family of 20 lowest-energy structures without significant distance viola-

Table 1: Structural Statistics and Atomic rms Deviations

Structural Statistics	{SA}[a]	⟨SA⟩r[b]
rms deviation from experimental constraints		
distance constraints (Å)[c]	0.008 ± 0.003	0.006
dihedral constraints (deg)[d]	0.15 ± 0.07	0.12
rms deviation from ideal geometry		
bonds (Å)	0.0028 ± 0.0001	0.0028
angles (deg)	0.53 ± 0.01	0.53
impropers (deg)	0.60 ± 0.06	0.58
no. of violations[e]		
distance constraints	58 ± 5	53
dihedral constraints	11 ± 2	11

rms Deviations from the Average Structure (Å)[f]	{SA}[a]
backbone (N−Cα−C′)	0.49 ± 0.07
side chains (heavy atom)	1.28 ± 0.14

[a] {SA} is the family of final 20 simulated annealing structures; mean values and standard deviations are shown for these 20 structures. [b] ⟨SA⟩r is the structure obtained by applying 10 000 steps of restrained minimization to the mathematical average structure. The mathematical average structure was obtained by first aligning the 20 structures with a least-squares fit over the regular secondary structure (N−Cα−C′ fragments of residues 5−13, 21−25, 33−37, 73−76, and 82−84) and then averaging the atomic coordinates. [c] A total of 929 distance constraints were used in the structure calculation: 264 long-range ($|i - j| > 4$), 369 medium-range ($1 < |i - j| \leq 4$), 270 intraresidue, and 13 × 2 H-bonds. [d] A total of 51 dihedral constraints were used in the structure calculation: 34 backbone φ angles and 17 side chain χ_1 angles. [e] All distance violations are less than 0.45 Å, and all dihedral violations are less than 1.4°. [f] The rms deviations of the atomic positions were calculated for each structure in {SA} against the mathematical average structure. The average values and standard deviations for the 20 final structures are reported when fitting over the ranges listed in footnote b. The rmsd for backbone atoms over the region of residues 3−88 is 2.2 ± 0.4 Å, which reflects the lack of definition in the heme-binding loop.

tions (all ≤0.45 Å and most ≤0.1 Å as reported by X-PLOR) was selected for Figure 2. Structures and restraints were analyzed with the programs AQUA and PROCHECK (*49*). The checking facility of the program WHAT IF (*50*) was used to compare the calculated structures with a set of high-resolution protein structures and to identify unusual geometries in the backbone and side chains. Regions of the structure remain imperfect because of a lack of restraints. For example, the backbone dihedral angles at Lys14 and Lys72 are abnormal.

Static Solvent Accessibility Calculations. Solvent-accessible surface areas (ASA) were calculated with the Lee and Richards algorithm (*51*) as implemented in the program Naccess (*52*). Standard van der Waals radii (*53*) and a probe radius of 1.4 Å were used. The backbone contribution of each amino acid was defined as the sum of the ASA's from the N, Cα, C′, and O atoms. Side chain contributions arose from all other atoms. Fractional accessibility estimates were obtained by dividing the absolute ASA's by the corresponding unfolded state values reported by Rose and co-workers (*54*). Upper and lower estimates were determined. Calculations were repeated over a family of 20 apoprotein structures. As an indicator of reliability, the results were averaged and the standard deviations were used, large values implying a fluctuating conformation and inaccurate information. The average NMR structure of rat ferrocyt b_5 (PDB entry 1aqa; *55*) was used for the holoprotein calculations.

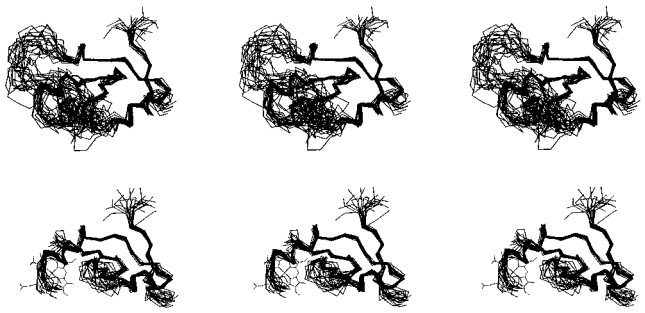

FIGURE 2: NMR structure of apocyt b_5. A total of 20 Cα traces are superimposed onto their geometrical average. The heme-binding site (elements α2, α3, β5, α4, and α5) is well defined only in α2 and the last turn of α5. The remainder is termed the heme-binding loop in the text. In the top triptych, the segment spanning residues 1−87 is depicted with the N-terminus pointing up and the C-terminus to the right. When viewed in stereo, the disordered heme-binding loop should appear behind the plane of the paper. The second triptych presents the same structures without the loop of residues 43−69. The orientation is slightly different and shows the heme group added where found in the holoprotein. Note helix α6 to the right, which undergoes a slow conformational exchange (milliseconds) in the apoprotein. The NMR restraints used in α6 were those corresponding to the helical conformation.

RESULTS

Structural Refinement. The previously determined low-resolution structure of rat hepatic apocyt b_5 (*1*) provides a good representation of folded elements. However, the heme-binding loop adopts a range of conformations that resist ready description. Triple-resonance experiments were performed to increase the number of distance restraints and confirm the partially folded nature of the loop. The inclusion of ^{13}C data resolved most remaining ambiguities and improved the quality of the structure. Although underdetermination still affects residues near and in the loop and leads to a few unlikely backbone dihedral angles, the improvement helped to elucidate the conformations sampled by the heme-binding loop and to define the extent of structural rearrangement imposed by the heme group. Statistical information is listed in Table 1.

Figure 2 presents an overlap of 20 Cα traces. As previously reported, several elements of structure are folded in the absence of the heme. These are, in sequence order, strand β1 (residues 4−7), helix α1 (residues 9−14), strand β4 (residues 21−25), strand β3 (residues 28−32), helix α2 (residues 33−38), the last turn of helix α5 (residues 70−74), strand β2 (residues 74−79), and the first turn of helix α6 (residues 80−84). The other elements of structure define the heme pocket and do not appear to be stably folded. Weak NOEs between strand β5 (residues 51−54) and strand β4 indicated that sampling of the holoprotein conformation does occur in this region. The calculations captured an occasional turn in the α3 region and no structural preference in α4, the helix of lowest local propensity according to its composition and the program AGADIR (*56*).

Thermodynamic Consequences of TMAO Addition. Apocyt b_5 undergoes a reversible two-state thermal denaturation that can be followed through the change in absorbance at 285 nm. The main contributor at this wavelength is Trp22, in the folded region of the structure (strand β4). The unfolding curves obtained by this method coincide with those produced

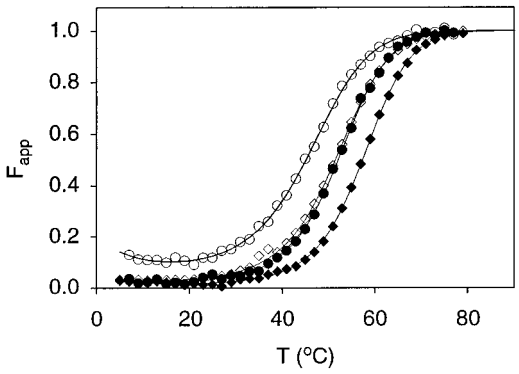

FIGURE 3: Thermal denaturation of apocyt b_5 monitored by UV−vis spectroscopy at different pHs and TMAO concentrations. The lines through the data points represent fits to a two-state process. Using the fitted thermodynamic parameters listed in Table 2, the fraction of unfolded apoprotein (F_{app}) was calculated as a function of temperature for the various conditions, which were (○) pH 7.3 and no added TMAO, (◇) pH 6.8 and no TMAO, (●) pH 7.3 and 0.9 M TMAO, and (◆) pH 6.8 and 0.9 M TMAO.

Table 2: Effect of TMAO on the Thermodynamic Parameters of Apocyt b_5[a]

	no TMAO		0.9 M TMAO	
	pH 6.8	pH 7.3	pH 6.8	pH 7.3
T_m (°C)	51.4 ± 0.1	45.0 ± 0.8	57.2 ± 0.4	52.0 ± 0.4
$\Delta H°(T_m)$ (kJ/mol)	145 ± 1	118 ± 8	173 ± 6	157 ± 7
$\Delta C_p°$ (kJ mol^{-1} K^{-1})	3.7 ± 0.1	4.0 ± 0.6	4.4 ± 0.3	4.6 ± 0.5
$\Delta G°$(25 °C) (kJ/mol)	7.7 ± 0.3	4.8 ± 0.3	9.7 ± 1.1	7.8 ± 1.2

[a] The uncertainties are the standard deviations of the fit except in the case of $\Delta G°$(25 °C), where a range was calculated with the deviations on $\Delta H°(T_m)$ and $\Delta C_p°$. The data correspond to those shown in Figure 3. Reproducibility trials demonstrated an uncertainty in $\Delta G°$(25 °C) reaching 30%.

by circular dichroism after normalization (*14*). Denaturation curves at two pH values (7.3 and 6.8) are shown in the absence and presence of TMAO in Figure 3. The corresponding thermodynamic parameters obtained through two-state fits are listed in Table 2. Apocyt b_5 is marginally stable under all conditions, with decreasing apparent $\Delta G°_{N\rightarrow U}$ at increasing pH. TMAO at a concentration of 1 M increased the midpoint of the transition (T_m) by a few degrees Celsius. A stabilization of the native state by 2−3 kJ/mol at 25 °C relative to the unfolded state was also observed, with the caveat that these small quantities are prone to error. The standard Gibbs energy values reported in the table indicate that at pH 7.3 and 25 °C, ∼90% of the protein is in the folded state, and that addition of 1 M TMAO increased this proportion to more than 95%.

Conformational Consequences of TMAO Addition. Upon addition of 1 M TMAO, the far-UV CD spectrum of apocyt b_5 exhibited a shift of the minimum from 203 to 206 nm accompanied by a small decrease in signal magnitude. These changes were qualitatively consistent with a conversion of random into regular structure but were much less pronounced than documented in instances of osmolyte-induced refolding (*22*).

^{1}H and ^{15}N assignments were verified in the presence of TMAO with 3D ^{1}H−^{15}N NOESY-HSQC and 3D ^{1}H−^{15}N TOCSY-HSQC data collected at pH 7.3. The analysis of these and homonuclear spectra indicated that the main features of the apoprotein state in aqueous solution, e.g., the

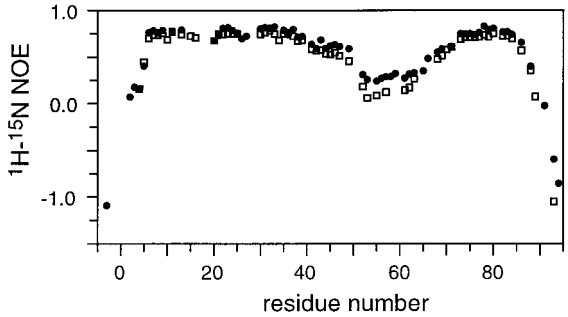

FIGURE 4: Effect of TMAO on the backbone dynamics of apocyt b_5 as shown by ^{1}H−^{15}N NOE values measured at 25 °C. Standard deviations are ∼8% (*15*). The data for the sample with 0.9 M TMAO at pH 7.3 are shown with the black circles (●), and the data at pH 7.7 in the absence of TMAO are shown with the white squares (□). The lower NOE values in the heme-binding loop and the termini correspond to the absence of structure in these parts of the backbone.

folded module and the disordered heme-binding loop, were maintained in 1 M TMAO. Chemical shift changes induced by TMAO demonstrated a small systematic upfield trend in the ^{1}H dimension. Values outside of two standard deviations from the average were observed in helix α3 and suggested that this region was susceptible to conformational shifts. A conformational shift was also noticed in helix α6, where the manifestation of slow exchange was largely attenuated. Overall, the appearances of the spectra were sharper with TMAO, suggesting a generalized restriction in the sampling of conformational space caused by the additive.

To confirm the minimal influence of TMAO on the heme-binding loop, the rapid segmental motions of the backbone were inspected by ^{1}H−^{15}N NOE measurements. Figure 4 compares data obtained with and without the osmolyte. Under both conditions, the NOE depression characteristic of accelerated motions in the heme-binding loop was apparent. A slight change in NOEs toward more positive values was observed upon addition of the osmolyte. This was attributed to an increase in bulk viscosity in the folded regions and local conformational changes affecting the amplitude of oscillations and correlated internal motions in the heme-binding loop. The addition of TMAO has an effect similar to cooling the solution by ∼10 °C (*15*).

Backbone Amide Proton Exchange. In apocyt b_5, a majority of amide backbone protons exchange with bulk solvent within the few minutes required to dissolve the protein in ^2H_2O and prepare the spectrometer for data collection (*1*, *27*). At pH 6.7 and 25 °C, exceptions are Tyr7 in strand β1, Glu11, Ile12, and Gln13 in helix α1, Val23 and Leu25 in strand β4, Val29 in strand β3, Phe35 in helix α2, and Ile76 in strand β2. The side chains of Tyr7, Val29, and Ile76 belong to hydrophobic core 2 in the β barrel, whereas Val23, Leu25, and Tyr35 belong to hydrophobic core 1. All these positions participate in stable secondary structure. On the basis of these data, the slowest rates of exchange are on the order of 10^{-3} s^{-1}. Under the same conditions, the rate constant for exchange in an unstructured polypeptide (k_{rc}) ranges between 2 and 200 s^{-1} following the calculations of Bai and co-workers (*41*).

Saturation transfer experiments were performed to map the rate of exchange along the backbone and probe motions slower than those previously described with ^{15}N relaxation data. According to eq 1, the ability to measure exchange

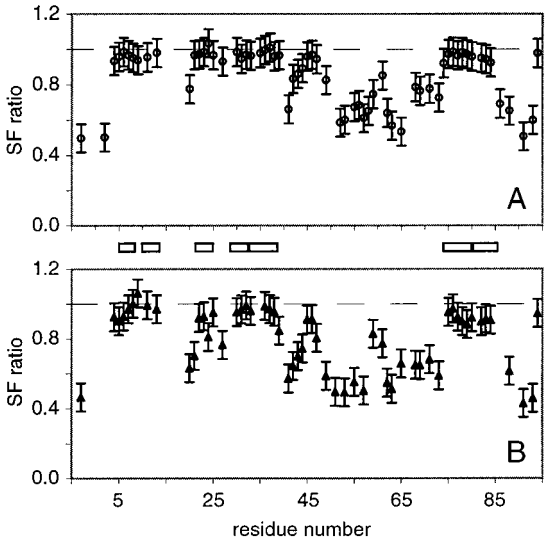

FIGURE 5: Ratio of saturation factors for apocyt b_5. Panel A shows the SF(pH 7.3; 0.9 M TMAO)/SF(pH 6.7; 0.9 M TMAO) ratio to illustrate the effect of pH. Panel B shows the SF(pH 7.3)/SF(pH 7.3; 0.9 M TMAO) ratio to illustrate the effect of TMAO. Error bars are set to ±0.08 estimated from error propagation and reproducibility. The C-terminal residue (Leu94) has a high value likely because of its low intrinsic rate. Horizontal bars between the two panels indicate the location of secondary structure in the apoprotein.

rates by the saturation transfer method depends on the relative values of ρ (the selective longitudinal relaxation time, generally approximated by the nonselective value) and k_{ex}, the observed rate constant. The average nonselective value was determined to be $\sim 0.3\ s^{-1}$, which implied that the saturation factor (SF) would vanish if $k_{ex} \gg 3\ s^{-1}$ and become unity if $k_{ex} \ll 0.03\ s^{-1}$.

In loops and termini, a number of amide hydrogens exhibited SF values between 0.2 and 0.8. In contrast, SF's for amide hydrogens participating in stable secondary structure at pH 6.7 were larger than 0.8. Hydrogens that exchange slowly according to the manual mixing experiment were not distinguishable within this set, suggesting that these hydrogens had reached the lower limit of k_{ex} that can be accessed by the saturation transfer method. In general, k_{ex} is expected to depend on the pH of the solution (*57*, *58*), and the experiment was repeated at pH 7.3 to test the validity of the above interpretation. Unchanged SF values would confirm that the rates are too slow to be measured.

Amide hydrogen exchange is both base- and acid-catalyzed, and k_{rc} (the rate in an unstructured peptide) is a function of pH expressed by

$$\frac{k_{rc}(pH_1)}{k_{rc}(pH_2)} = 10^{pH_2 - pH_1} \quad (4)$$

Equation 4 shows that an ~4-fold rate enhancement in the chemical step will occur at pH 7.3 versus pH 6.7. In addition to this intrinsic contribution, the denaturation data in Figure 3 showed that near neutral pH, the stability of the native state of apocyt b_5 decreased as the pH was increased. Native state destabilization may contribute to rate enhancement at the higher pH. Figure 5A illustrates the ratio of saturation factor obtained at the two pH values versus residue number in the presence of 0.9 M TMAO. In the structured regions, this ratio was close to unity, indicating that pH effects were not detected by the method. In contrast, the hydrogens for which the saturation factors were between 0.2 and 0.8 were sensitive to pH. The same observations held in the absence of TMAO. Figure 5B depicts the ratio obtained at pH 7.3 with and without TMAO. The TMAO effect on the unstructured regions was comparable to the pH effect.

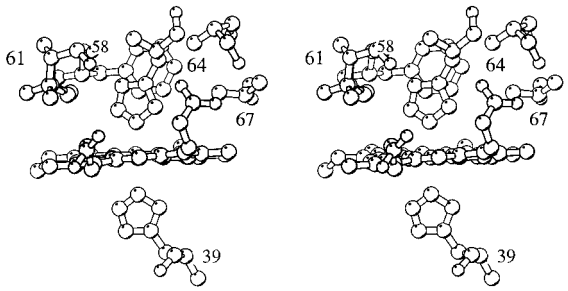

FIGURE 6: Environment of His63 in the wild-type holoprotein (stereoview made from PDB entry 1cyo). Phe58 is located behind the coordinated His63. The side chain of Val61 is disordered in the solid state structure and is shown with two orientations of the isopropyl group. The propionate substituent at heme position 7 points up to form a H-bond with the backbone NH of Ser64.

The hydrogen-exchange results are summarized in three observations. First, the few amide hydrogens protected from exchange so as to remain detectable within minutes of dissolution in ^2H_2O belong to regions of the structure where there is systematic retardation. In fact, all protons identified in the secondary structure of apocyt b_5 exhibited slow exchange compared to the unstructured peptide under the same conditions of pH and temperature. Second, there was little protection in the heme-binding loop, in agreement with the multiple conformations rapidly sampled by this segment of the protein. Finally, the limitations of the saturation transfer method are such that the effect of the osmolyte on the exchange rates in the structured regions could not be detected. In the heme-binding loop, where the method is adequate, TMAO was found to have no significant effect, in line with its inability to induce lasting structure in this region of the protein.

Lasting structure is imposed by the heme, which has several types of interactions with the protein matrix: van der Waals contacts, electrostatic interactions, and coordination bonds with each of the axial histidines. The next section inspects the consequences of reducing the affinity for the heme group. It also addresses the importance of the ligation to His63 in refolding the mobile loop and in the propagation of conformational changes through the protein. Figure 6 shows the environment of His63 in the structure of the holoprotein.

Properties of Apo H63A Cytochrome b_5. To interpret the data collected on heme-bound H63A cyt b_5, it was necessary to establish whether the apoprotein was affected by the side chain replacement. The global fold of the apoprotein was inspected by CD in the far-UV region at 25 °C. The spectra of the wild-type and variant apoproteins were not significantly different and are not shown. The thermal denaturation of the variant was followed at pH 6.7 as described above for the TMAO studies. In this case as well, the normalized plots obtained with a two-state treatment of the data collected on the wild-type and variant apoproteins were indistinguishable and demonstrated that the mutation did not affect the

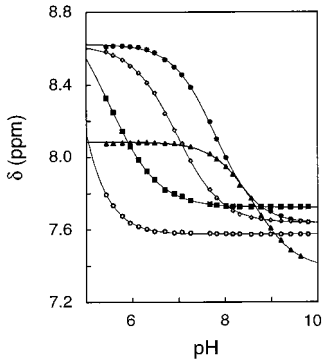

FIGURE 7: pH titration of H63A apocyt b_5 in ^2H_2O. The data points are from the CϵH signals of His15 (▲), His26 (◇), His27 (■), His39 (●), and His80 (○). The lines represent fits to a modified Henderson−Hasselbalch equation; pK values are listed in Table 3.

Table 3: Histidine Ionization Constants in Apocyt b_5[a]

residue	wild type[b]	H63A
His15	8.50	8.64
His26	6.90	6.95
His27	between 5 and 6	between 5 and 6
His39	7.68	7.78
His63	7.36	−
His80	<5.5	<5.5

[a] Measured in 99% ^2H_2O; values uncorrected for isotope effects. [b] Average value for the CδH and CϵH, taken from ref *45*. Experimental values have an estimated uncertainty of 0.1; in all cases, the standard deviation of the fit is <0.1.

global stability of the native state or the cooperativity of the unfolding transition.

A pH titration of the apoprotein was performed to characterize the influence of the replacement at position 63 on the ionization equilibrium of the remaining axial His39. This was a required control because heme binding takes place by coordination of the iron ion to the Nϵ atom of the axial histidine in the neutral state. The titration curves are shown in the chemical shift versus pH plot of Figure 7, and the pK values are reported in Table 3. In the wild-type protein, His39 has an apparent pK_a of 7.6 (*45*). In H63A apocyt b_5, His39 maintained the same ionization constant.

It is conceivable that a minor change in structure, important for heme binding, may not give rise to a marked change in the CD spectrum or in the stability of the folded module. ^1H NMR data were collected to explore this possibility. Although the assignments in H63A apocyt b_5 were not as complete as in the wild-type protein where isotopic labels were used, they were sufficient to construct a plot of chemical shift differences to test structural similarity. This plot is shown in Figure 8. Aside from expected chemical shift changes near the site of mutation, no significant variation was detected, and it was concluded that there was no major modification of structure in the heme-binding loop and elsewhere.

Properties of Reduced H63A Cytochrome b_5 Complexed with Carbon Monoxide. H63A apocyt b_5 was found to bind heme, albeit with a low affinity. NMR data were collected on the ferric complex ligated with cyanide and the ferrous complex ligated with carbon monoxide. In both cases, spectra were of good quality. The ferric complex was less stable than the reduced complex, likely because of the ionic

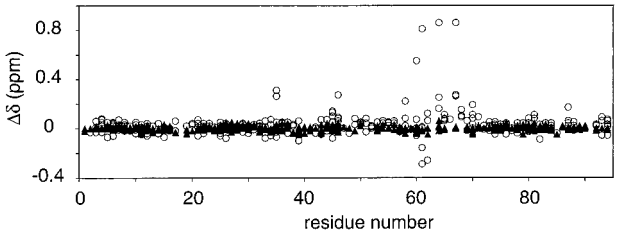

FIGURE 8: Effect of the H63A replacement on the chemical shifts of the apoprotein (▲) and the holoprotein (○). The difference is plotted vs residue number. A total of 370 chemical shift values are represented for the apoprotein. The standard deviation of this ensemble is 0.02 ppm. A total of 300 values are plotted for the holoprotein.

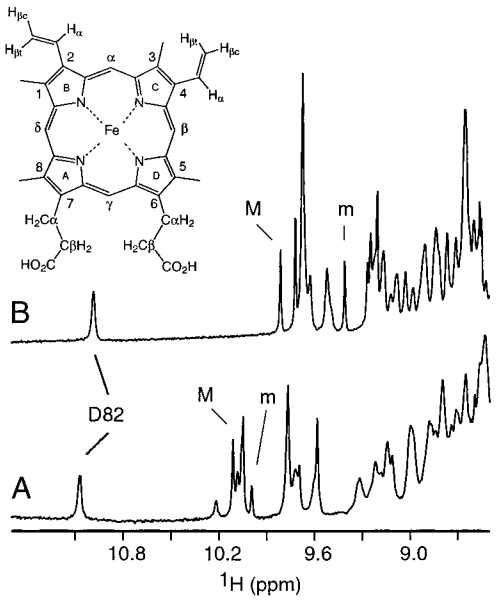

FIGURE 9: Downfield spectral region of rat holocyt b_5 in 90% H_2O and 10% ^2H_2O at pH 7.4 and 25 °C. Trace A represents the CO complex of reduced H63A and trace B reduced wild-type cyt b_5. M and m indicate lines from the major and minor heme isomers, respectively. D82 points to the backbone NH of Asp82, which forms an N-terminal helix capping H-bond with His80. The inset shows the nomenclature for the heme group.

character of the ligation bond (*59*), and the ferrous form was chosen for further study.

Figure 9 compares the downfield region of the 1D spectrum of wild-type ferrocyt b_5 and H63A ferrocyt b_5-CO. The appearance of the second spectrum is that of a diamagnetic species with heme specifically bound to the polypeptide matrix. The resonances of the heme (structure and nomenclature in the inset of Figure 9) were assigned using typical connectivities (*60*); for example, the signals of the vinyl side chains were identified by their unique correlation pattern in the aromatic region. Each vinyl group had NOEs to a downfield-shifted meso proton and a heme methyl group near 3 ppm. Further assignments relied on the unique position of the δ meso proton between methyl group 1, adjacent to a vinyl side chain, and methyl group 8, adjacent to a propionate side chain.

As in the wild-type holoprotein, two sets of heme resonances were observed, termed M and m. The origin of these two wild-type forms is heme rotational isomerism, which involves a 180° rotation of the heme about its $\alpha-\gamma$ meso axis in the protein cavity (*61*). In H63A cyt b_5, the heme β-meso proton in the major isomer was found to be in

Table 4: Chemical Shift of Heme Resonances in H63A Cyt b_5-CO[a]

	major form	minor form		major form	minor form
α-meso	9.57	9.69	8-CH_3	3.64	3.61
β-meso	10.03	9.98	2-α vinyl	7.37	7.89
γ-meso	9.75	9.77	2-β vinyl	5.45	6.17
δ-meso	10.10	10.05	2-β vinyl	5.28	5.72
1-CH_3	3.37	3.46	4-α vinyl	8.25	8.40
3-CH_3	3.32	2.92	4-β vinyl	6.00	
5-CH_3	3.60	3.59			

[a] Measured in 90% H_2O and 10% ^2H_2O at pH 7.4 with 20 mM Tris at 25 °C.

Table 5: Selected Chemical Shifts for H63A Cyt b_5-CO[a]

residue		major form[b]	wild type[c]	rc difference[d]	rcs[e]
Val61	NH	6.73	6.73	−1.71	−0.8
	αH	3.29	3.30	−0.9	−0.4
	βH	0.56	0.40	−1.57	−0.2
	γCH_3	−0.78	−1.07	−1.75	−1.9
	γCH_3	−0.03	0.78	−0.97	0
Ala63	NH	6.61	−	−1.6	−1.6
	αH	2.61	−	−1.7	−2.0
	βCH_3	−0.88	−	−2.3	−2.9
Ala67	NH	8.27	8.54	0.02	0
	αH	4.48	4.74	0.13	0.7
	βCH_3	0.37	1.23	−1.03	−0.8

[a] Measured in 90% H_2O and 10% ^2H_2O at pH 7.4 with 20 mM Tris at 25 °C. [b] Only the major isomer signals are listed. [c] Wild-type data collected under similar conditions; assignments as in ref *17*. [d] Difference between the random coil value (*89*) and the value in H63A cyt b_5. [e] Ring current shift due to the heme group calculated with the wild-type structure (PDB entry 1cyo).

dipolar contact with a methyl group from a valine residue, identified as Val61. Val61 exhibited two well-resolved sets of resonances. The minor Val61 set exhibited NOEs to the δ-meso proton of the second heme form as expected with a 180° rotation of the heme. Heme chemical shifts are listed in Table 4.

Previous work has shown that the spectral properties of cyt b_5 regions both remote from the heme-binding site and folded in the apoprotein are moderately sensitive to heme removal (*27*). A lesser perturbation of the heme site, such as from the H63A replacement, was therefore expected to cause minor spectral changes in the same regions. The corresponding subspectra indeed bore a high degree of resemblance to those in the wild-type holoprotein; many assignments could be transferred from one protein to the other and readily confirmed with analysis of ^{1}H-correlated and NOESY data. For the regions closer to the heme group, analysis started with Ala63, an additional, conspicuously upfield-shifted alanine (Table 5). Other assignments were obtained either by starting from residues giving rise to the spectrally similar regions or directly from the heme group. For example, the δ-meso proton and the 8-methyl group in the major species had NOEs to a shifted alanine residue. This was assigned as Ala67 on the basis of the wild-type structure (Figure 6) and confirmed with sequential connectivities. Intermethyl NOEs between Ala63 and Ala67 in both the major and minor isomers and Val61−heme NOEs supported the collapse of the heme-binding loop onto the heme group as in the wild-type structure. Thus, coordination to His63 was not required for the refolding of the structure; the entropic cost of organizing the polypeptide chain was

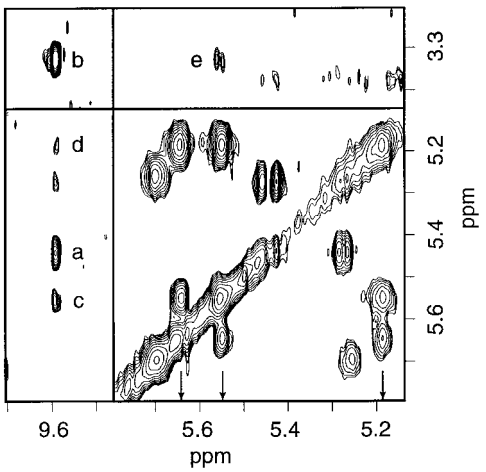

FIGURE 10: Sections of the ^{1}H−^{1}H 2D spectrum collected in 90% H_2O and 10% ^2H_2O on reduced H63A cyt b_5, complexed with CO at pH 7.4 and 25 °C. The panel containing the diagonal is from a TOCSY data set. The cross-peaks appearing at combinations of 5.18, 5.54, and 5.64 ppm arise from the major form of Phe58. The surrounding panels are from a NOESY data set. The signal at ~9.6 ppm arises from the α-meso proton. Cross-peaks a−d are due to this meso proton in contact with one of the 4-β vinyl, heme 3-CH_3, Phe58 δ, and Phe58 ϵ protons, respectively. Cross-peak e is between Phe58 ϵ protons and the heme 3-CH_3.

offset by favorable interactions with the heme group. A strong NOE effect between the α and β protons of Ala63 and the amide NH of Ser64 suggested extended structure in this region, as seen between helices α4 and α5 in the wild-type protein (Figure 1).

An interesting difference between the wild-type and the H63A holoprotein is illustrated in Figure 10, which contains a portion of a TOCSY data set (diagonal panel) surrounded by sections from a NOESY experiment. The TOCSY data displayed an AMX spin system reminiscent of a phenylalanine ring at 5.18, 5.54, and 5.64 ppm. The 2QF-COSY pattern was consistent with this interpretation and placed the ring ϵ protons at 5.18 ppm. NOEs indicated that this system was near the α-meso proton and the 3-methyl group and suggested assignment to Phe58, a residue in contact with His63 in the wild-type protein (Figure 6). When a histidine occupies position 63 and an alanine occupies position 67, the ring of Phe58 does not rotate freely about its $\gamma-\zeta$ axis, and the ring δ and ϵ resonances are severely broadened (*62*). The replacement of His63 with the smaller Ala63 removed the steric hindrance. The chemical shifts reported in the wild-type cytochrome for the ϵ and ζ protons (*62*) are consistent with those observed here. A similar dynamic alteration has been reported in A67V cyt b_5 (*63*).

The similarity between H63A ferrocyt b_5-CO and wild-type ferrocyt b_5 is not immediately visible in Figure 9 because the heme resonances, which dominate this chemical shift window, occur at markedly different frequencies. However, the above analysis of the ^{1}H-correlated and NOESY data revealed that most protein signals were minimally shifted by the amino acid replacement and altered coordination (Figure 8). Outliers were located mainly on the position 63 side of the heme. In particular, Val61 and Ala67 underwent a significant chemical shift change reflecting rearrangement of the loop with respect to the heme plane. It should be emphasized that the shifts were not systematically toward random values, supporting a different but folded structure.

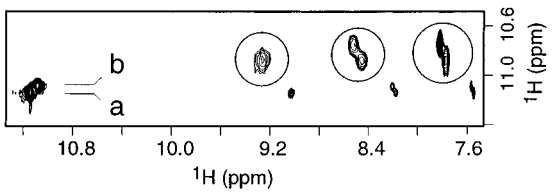

FIGURE 11: Section of a NOESY spectrum collected on an equimolar mixture of H63A cyt b_5 in the apo form and the reduced CO form at pH 7.5 and 25 °C. Peaks a and b are diagonal peaks arising from the apoprotein and the holoprotein, respectively. The insets in circles enlarge the cross-peaks in this region of the spectrum. Only the apoprotein displays a cross-peak at 9.2 ppm, identified as an exchange cross-peak in the TOCSY data.

On the other side of the heme, the residues that experienced a shift compared to the wild type were Phe35 and Leu46. Phe35 had NOEs to the axial His39 α and β protons as well as the heme δ-meso proton as in the wild-type protein. Leu46 was found to be in contact with the 3-methyl and the α-meso proton. Thus, it is likely that the differences in shifts were due to a reorientation of the heme group within its cavity.

Support for an altered heme orientation in H63A cyt b_5 is provided in Figure 9 and 2D data. In equilibrated wild-type protein samples, the ratio of the two heme orientational isomers, identified by M (major) and m (minor) in Figure 9, is ~55:45 (*64*). In the H63A holoprotein (reduced, CO bound), the ratio was 75:25, determined by integration of resolved 1D lines or cross-peak volume measurements. Comparison of cytochromes from various natural sources and with engineered amino acid replacements has identified a few key interactions in the control of the equilibrium proportions. Most notable are the hydrophobic residues located at positions 23 and 74 (*62*, *65*), both in contact with the heme group, and the backbone NH of Ser64, which forms a H-bond with one of the heme propionate side chains in the major isomer (*17*). Besides these enthalpic contributions, less predictable entropic terms are expected to dictate the outcome of replacements (*62*). The increased proportion of the major isomer obtained with the H63A protein may be related to a reorientation of the position 64 NH as the removal of the coordination bond should allow the backbone to relax into a different conformation.

Finally, the conformational exchange in α6 was used to assess the long-range dynamic consequences of heme binding in H63A cyt b_5. This exchange process involves capping and uncapping at the helix N-terminus and is readily detected with the backbone amide hydrogen of Asp82 at ~11 ppm. In the capped, folded form, the Asp82 NH has an NOE to the NH of Asp83 and the CϵH of His80. The occurrence of conformational exchange on the millisecond time scale is manifested by a ROESY, TOCSY, and NOESY cross-peak at a chemical shift of ~9 ppm, marking the second environment of the Asp82 NH. Other exchange cross-peaks are identified along α6 in the amide region. Whereas the wild-type apoprotein contains a small population of uncapped α6 in exchange with the folded form, heme binding quenches the process (*19*).

Figure 11 presents NOESY data collected on a sample of H63A apocyt b_5 to which a substoichiometric amount of hemin was added. Subsequent reduction with dithionite and addition of CO resulted in a solution containing nearly equimolar amounts of apoprotein and diamagnetic holoprotein, as determined by the relative areas of Asp82 NH resonances at 11 ppm (Asp82 NH resonances are conveniently separated by ~0.1 ppm in the folded apo and holo forms). The advantage of this sample was that holoprotein and apoprotein data were collected under strictly identical conditions. Exchange processes were unambiguously identified in TOCSY experiments; NOESY data are presented here to illustrate additional cross-peaks. In the apoprotein form (designated with an a in Figure 11), three cross-peaks were observed in the aromatic region. They corresponded to the expected NOE connectivities to Asp83 and His80 and to chemical exchange with the Asp82 NH in the second conformation. In the holoprotein form (b in Figure 11), only the two NOE cross-peaks were detected. None of the other exchange cross-peaks seen along α6 were observed. Thus, it appeared that ligation of the heme by His39 and refolding of the heme-binding loop were sufficient to reduce the conformational freedom of α6 and to relay the heme binding status to this remote region of the protein.

DISCUSSION

Mobile protein segments often participate in catalytic steps by recruiting residues to the active site of enzymes (*66*−*69*). Aside from this functional role, they influence the energetics of a native protein with large entropic contributions. In the case of refolding induced by prosthetic group binding, the conformational changes they undergo may modulate affinity as well as organize residues correctly for chemistry at the active site. Recently, another role has been proposed by which unstable structural elements facilitate the distribution of conformational readjustments away from the site upon binding (*10*, *70*). Exploring this proposal requires the alteration of specific interactions within the flexible regions and the means for monitoring the consequences of these alterations. Mobile segments are particularly challenging for experimental characterization, and here, several methods were applied to investigate the conformational shift involving the heme-binding loop of apocyt b_5.

The improved model of apocyt b_5 confirmed the stretch comprising residues 43−69 to be of low structural stability. Estimates of static accessible surface area (ASA) based on the holoprotein structure and 20 apoprotein structures revealed that upon removal of the heme group, the level of solvent exposure increased not only for the residues in contact with the group but also in regions packed against the elements that unfold. One such region is located at the connection between helix α1 and strand β4, which docks on helix α3 in the holoprotein (Figure 1). NMR structures capture the fluctuating apoprotein conformations imperfectly, and ASA calculations are bound to be less reliable in these ill-defined regions. Nevertheless, the ASA increase was clearly largest from residue 49 to 58 (EQAGGDATENFE). The effects of copper nitrilotriacetic acid (*45*) and HyTEMPO (*71*) on the NMR spectrum provide additional evidence that this region is exposed to solvent.

Backbone amide-exchange data were collected to complement the dynamic representation obtained with nuclear relaxation approaches (*15*). Hydrogen-exchange results are generally interpreted with EX1 or EX2 mechanisms (*57*, *58*). These are derived for stable proteins where the rate at which the structure opens to allow exchange (rate constant k_{op}) is

much slower than the rate at which it closes (rate constant k_{cl}). For apocyt b_5 at pH 6.8, the apparent equilibrium constant pertaining to global unfolding, or k_u/k_f, is $\sim^1/_{24}$ (Table 2). The rate of global refolding of the rat apoprotein (k_f) can be estimated at pH 6.8 and 25 °C with kinetic experiments performed from the urea-unfolded state (*27*, *72*). The value is lower than 100 s^{-1}, and consequently, the global unfolding rate constant (k_u) is lower than 4 s^{-1}. This makes k_u comparable to the calculated k_{rc}, and if k_u and k_f are taken to represent k_{op} and k_{cl}, respectively, apocyt b_5 is too unstable for the simplified equations to hold.[2] Thus, the interpretation of the H-exchange data was limited, but it confirmed that the folded and unfolded modules of the apoprotein had distinct signatures on all accessible time scales. When the heme is bound, the native state stability is high, and exchange rates vary from 10^{-3} to 10^{-9} s^{-1} at pH 7.0 and 40 °C (*17*). Interestingly, no correlation is observed between NH lifetime and location within hydrophobic cores 1 and 2 (*17*). Taken together, these and prior data showed that native apocyt b_5 contained three regions that can be distinguished by their conformational lability (helix α6, the remainder of the folded module, and the heme-binding loop), and that these distinctions were suppressed in the holoprotein.

All indicators agreed that the polypeptide chain could be organized more compactly than in the apoprotein; this suggested that an osmolyte might induce refolding and stabilize ordered conformations of the heme-binding loop. The additive TMAO at a concentration of 1 M was therefore tested for its ability to alter the three regions of apocyt b_5. The osmolyte was found to affect the energetics of protein denaturation to a measurable extent. The parameter most sensitive to TMAO was T_m, while $\Delta\Delta G°$ at 25 °C was small, a behavior documented for other osmolytes and proteins (*74*). The change in standard Gibbs energy difference between unfolded and native states caused by the osmolyte ($\Delta\Delta G°$ or $\Delta G°_{N,TMAO\rightarrow U,TMAO} - \Delta G°_{N\rightarrow U} = \Delta G°_{U\rightarrow U,TMAO} - \Delta G°_{N\rightarrow N,TMAO}$) can be estimated within a transfer free energy model with a weighted sum of side chain and backbone contributions (*75*). The weighting factor represents the fractional change in ASA upon unfolding. To obtain these factors, ASA values for the folded module were compared to upper and lower limits of the level of solvent exposure for its unfolded state (*54*). The contribution from the solvent-exposed loop was expected to cancel out, and was ignored. The calculations returned a change in $\Delta G°$ between 1 and 4 kJ/mol, accounting for the low experimental $\Delta\Delta G°$ values (Table 2).

The improved appearance of the NMR spectra of the folded module can be interpreted as modest perturbations of the conformational distribution within the native apoprotein ensemble. These perturbations are consistent with excluded volume effects (*76*), favoring compact substates (*77*) and the observation of increased native state population upon TMAO addition (Figure 3). In other regions of the protein, the improvement may have different causes, including the acceleration of fast conformational exchanges or the retardation of slow exchanges without population changes. The relationship between spectral appearance and dynamic properties (*78*) is too complicated to arrive at a conclusion without additional data. In any event, the use of TMAO may be advantageous in the NMR study of other proteins with a broad range of accessible conformations in a given thermodynamic state.

The manifestations of conformational exchange in helix α6 were strongly attenuated upon addition of TMAO. In this element as well, a likely cause is a population shift toward the folded form. This perturbation could either have a local origin (action of the osmolyte on the unfolded state of the helix) or stem from a global effect (action of the osmolyte on the folded module behaving as a cooperative unit). Action relayed from the distant heme site was ruled out since this portion of the protein was not affected by the change in solvent properties. That is, within the flexible loop, no major conformational response to the osmolyte was detected, and it appeared that interactions with a molecule such as the heme rather than preferential solvation effects were required to maintain the holoprotein geometry.

The heme group extends the cooperative network to the entire cyt b_5 structure and imposes major conformational shifts, with the 30-residue loop around His63 undergoing the largest rearrangement. This effect could be simply due to the covalent attachment of the axial residue and the ensuing structural strains. To investigate this possibility, His63 was replaced with an alanine. Replacement of an axial residue in a *b* hemoprotein has proven to be a useful tool for altering heme reactivity (*79*−*81*) and studying the kinetics of heme binding (*82*). The H63A replacement in rat liver cyt b_5 decreased the affinity for the prosthetic group drastically. This observation was not surprising in light of a prior report that H63A cyt b_5 did not bind heme (*79*).

Axial histidine replacement is particularly instructive in globins (*24*, *83*), where the detachment of the heme from the protein frame was found to increase the ligand affinity at the distal position and to reduce significantly the cooperativity of oxygen binding. In metmyoglobin (a ferric complex with water as the sixth iron ligand), the coordination bond energy is estimated to be ∼20 kJ/mol (*84*), an amount comparable to the free energy contribution of specific interactions between heme and contacting side chains. Nonspecific partitioning into the nonpolar heme cavity accounts for 30−40 kJ/mol. Given the higher polarity of the cyt b_5 heme cavity versus that of the myoglobin heme cavity, the nonspecific partitioning free energy contribution is expected to be inadequate for maintaining the heme within the cytochrome. This is illustrated by the unsuccessful attempts at preparing the complex between protoporphyrin IX (des-iron heme) and wild-type apocyt b_5 (*1*), whereas sperm whale apomyoglobin binds the metal-free prosthetic group and refolds (*85*, *86*).

By using a typical bimolecular heme binding rate constant of $\sim 10^8$ M^{-1} s^{-1} (*84*), a unimolecular rate constant for heme loss of $\sim 6 \times 10^{-5}$ s^{-1} (*87*), and experimental Gibbs energies of unfolding (*13*, *14*), an approximate energy diagram can be constructed for wild-type cyt b_5. This hypothetical diagram, along with that for H63A cyt b_5, is shown in Figure 12. Among the many factors that influence the energetics of the variant holoprotein state are the effect of CO on the strength of the remaining axial bond to His39 and the identity

[2] The acceleration of H-exchange rates caused by heme removal, however considerable, was lower in magnitude than expected solely on the basis of the global unfolding rate. At neutral pH, this may be due in part to the lack of access by the hydroxide ions responsible for base-catalyzed exchange (*73*) and in part to residual local structure.

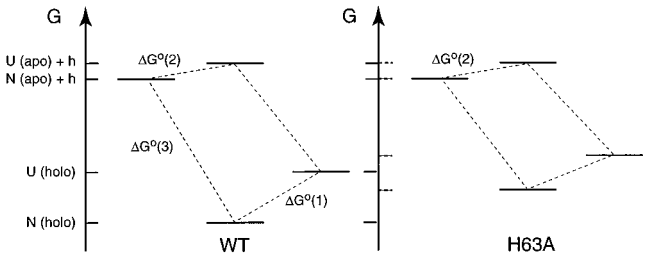

FIGURE 12: Schematic representation of the free energy changes associated with folding and heme binding in wild-type (WT) and H63A cyt b_5. Four thermodynamic states are indicated: N (holo), native holoprotein state; U (holo), unfolded protein with nonspecifically associated heme (e.g., as in cytochrome b_{562}; *90*); N (apo) + h, native apoprotein with free heme; and U (apo) + h, unfolded apoprotein with free heme. $\Delta G_1°$ (25 kJ/mol) and $\Delta G_2°$ (7 kJ/mol) represent the free energy of unfolding for the holoprotein and the apoprotein, respectively (*13*, *14*). $\Delta G_3°$ in the wild-type diagram is an estimate of the binding energy (70 kJ/mol) calculated under standard (1 M) conditions with a rate constant for binding of $\sim 10^8$ M^{-1} s^{-1} (*84*) and a unimolecular rate constant for heme loss of $\sim 10^{-5}$ s^{-1} (*87*). For the H63A diagram, $\Delta G_2°$ was as in the wild type (see the text). The lower heme affinity of H63A cyt b_5 compared to wild-type cyt b_5 is represented by an arbitrarily raised native holoprotein level. Nonspecific heme binding to the unfolded state was also weakened because of the removal of one histidine. The U (apo) + h levels for WT and H63A were arbitrarily set to the same free energy.

of the replacing side chain. H63A cyt b_5 has lower heme affinity than the H63M protein (*79*) and the H63L protein (*82*). The difference could be due to additional hydrophobic interactions with the bulky Met and Leu side chains and entropic contributions from changes in solvation. In contrast, the replacement of His39 with Ala (J. T. J. Lecomte et al., unpublished results) or Leu (*82*) results in a protein with higher affinity for the heme group than H63A cyt b_5 and argues for uneven contributions of the two axial residues, in part because of the higher energetic cost in refolding the loop without direct attachment to the heme.

The choice of alanine to replace the mobile axial histidine His63 and attenuate heme affinity provided clues to protein organization and the role of unstable structural elements. It revealed that as long as the prosthetic group was in its cavity, the refolding of the loop was complete. In this context, as in the folding of a single polypeptide chain, the specificity for the three-dimensional structure of the loop appeared to be largely decoupled from its stability. In addition, refolding in this region triggered conformational changes propagating the "heme-bound" information to the C-terminal helix. This transmission was independent of ligation and did not require tight binding of the heme, emphasizing again the importance of holoprotein conformation, rather than wild-type stability, in relaying these effects. Further dissection of the process will show whether a specific subset of residues mediates communication across the protein.

ACKNOWLEDGMENT

We thank Dr. C. Robert Matthews and the members of his research group for assistance with the collection of CD data and for numerous discussions. We are especially grateful to Dr. Jill Zitzewitz for technical advice and critical reading of the manuscript. We also thank Anthony Cabral for protein preparation. The ribbon diagram shown in Figure 1 was generated with MOLSCRIPT (*88*). The 14.1 T NMR spectrometer was purchased with a grant from the National Institutes of Health (S10 RR10524).

SUPPORTING INFORMATION AVAILABLE

Two tables listing the chemical shifts of the apoprotein. This material is available free of charge via the Internet at http://pubs.acs.org.

REFERENCES

1. Falzone, C. J., Mayer, M. R., Whiteman, E. L., Moore, C. D., and Lecomte, J. T. J. (1996) *Biochemistry 35*, 6519−6526.
2. Lecomte, J. T. J., Sukits, S. F., Bhattacharya, S., and Falzone, C. J. (1999) *Protein Sci. 8*, 1484−1491.
3. Feng, Y., Sligar, S. G., and Wand, A. J. (1994) *Nat. Struct. Biol. 1*, 30−35.
4. Tsai, C. J., Xu, D., and Nussinov, R. (1998) *Folding Des. 3*, R71−R80.
5. Lattman, E. E., and Rose, G. D. (1993) *Proc. Natl. Acad. Sci. U.S.A. 90*, 439−441.
6. Williams, D. C., Jr., Benjamin, D. C., Poljak, R. J., and Rule, G. S. (1996) *J. Mol. Biol. 257*, 866−876.
7. Engen, J. R., Gmeiner, W. H., Smithgall, T. E., and Smith, D. L. (1999) *Biochemistry 38*, 8926−8935.
8. McIntosh, P. B., Taylor, I. A., Frenkiel, T. A., Smerdon, S. J., and Lane, A. N. (2000) *J. Biomol. NMR 16*, 183−196.
9. Lee, A. L., Kinnear, S. A., and Wand, A. J. (2000) *Nat. Struct. Biol. 7*, 72−77.
10. Freire, E. (1999) *Proc. Natl. Acad. Sci. U.S.A. 96*, 10118−10122.
11. Mathews, F. S., and Czerwinski, E. W. (1976) *The Enzymes of Biological Membranes*, Vol. 4, Plenum Press, New York.
12. Teale, F. W. J. (1959) *Biochim. Biophys. Acta 35*, 543.
13. Pfeil, W. (1993) *Protein Sci. 2*, 1497−1501.
14. Constans, A. J., Mayers, M. R., Sukits, S. F., and Lecomte, J. T. J. (1998) *Protein Sci. 7*, 1983−1993.
15. Bhattacharya, S., Falzone, C. J., and Lecomte, J. T. J. (1999) *Biochemistry 38*, 2577−2589.
16. Kelly, G. P., Muskett, F. W., and Whitford, D. (1997) *Eur. J. Biochem. 245*, 349−354.
17. Dangi, B., Sarma, S., Yan, C., Banville, D. L., and Guiles, R. D. (1998) *Biochemistry 37*, 8289−8302.
18. Banci, L., Bertini, I., Cavazza, C., Felli, I. C., and Kouloughliotis, D. (1998) *Biochemistry 37*, 12320−12330.
19. Lecomte, J. T. J., and Moore, C. D. (1991) *J. Am. Chem. Soc. 113*, 9663−9665.
20. Fuentes, E. J., and Wand, A. J. (1998) *Biochemistry 37*, 3687−3698.
21. Baskakov, I., and Bolen, D. W. (1998) *J. Biol. Chem. 273*, 4831−4834.
22. Baskakov, I. V., Kumar, R., Srinivasan, G., Ji, Y. S., Bolen, D. W., and Thompson, E. B. (1999) *J. Biol. Chem. 274*, 10693−10696.
23. Wang, A., and Bolen, D. W. (1997) *Biochemistry 36*, 9101−9108.
24. Barrick, D. (1994) *Biochemistry 33*, 6546−6554.
25. Schmid, F. X. (1989) in *Protein Structure. A Practical Approach* (Creighton, T. E., Ed.) pp 251−285, IRL Press, New York.
26. Live, D. H., Davis, D. G., Agosta, W. C., and Cowburn, D. (1984) *J. Am. Chem. Soc. 106*, 1939−1941.
27. Moore, C. D., and Lecomte, J. T. J. (1993) *Biochemistry 32*, 199−207.
28. Kay, L. E., Xu, G.-Y., Singer, A. U., Muhandiram, D. R., and Forman-Kay, J. D. (1993) *J. Magn. Reson., Ser. B 101*, 333−337.
29. Muhandiram, D. R., and Kay, L. E. (1993) *J. Magn. Reson., Ser. B 102*, 317−321.
30. Kay, L. E., Ikura, M., Tschudin, R., and Bax, A. (1990) *J. Magn. Reson. 89*, 496−514.
31. Bax, A., and Ikura, M. (1991) *J. Biomol. NMR 1*, 99−104.
32. Grzesiek, S., and Bax, A. (1992) *J. Magn. Reson. 99*, 201−207.

33. Marion, D., Ikura, M., Tschudin, R., and Bax, A. (1989) *J. Magn. Reson. 85*, 393−399.
34. Piotto, M., Saudek, V., and Sklenăr, V. (1992) *J. Biomol. NMR 2*, 661−665.
35. Sklenăr, V., Piotto, M., Lepik, R., and Saudek, V. (1993) *J. Magn. Reson. 102*, 241−245.
36. Skelton, N. J., Palmer, A. G. I., Akke, M., Kördel, J., Rance, M., and Chazin, W. J. (1993) *J. Magn. Reson., Ser. B 102*, 253−264.
37. Shaka, A. J., Keeler, J., and Freeman, R. (1983) *J. Magn. Reson. 53*, 313−340.
38. Lyons, T. A., Ratnaswamy, G., and Pochapsky, T. C. (1996) *Protein Sci. 5*, 627−639.
39. Neuhaus, D., and Williamson, M. (1989) *The nuclear Overhauser effect in structural and conformational analysis*, VCH, New York.
40. Gryk, M. R., Finucane, M. D., Zheng, Z., and Jardetzky, O. (1995) *J. Mol. Biol. 246*, 618−627.
41. Bai, Y., Milne, J. S., Mayne, L., and Englander, S. W. (1993) *Proteins 17*, 75−86.
42. Mori, S., Johnson, M. O., Berg, J. M., and van Zijl, P. C. M. (1994) *J. Am. Chem. Soc. 116*, 11982−11984.
43. Mori, S., Abeygunawardana, C., van Zijl, P. C. M., and Berg, J. M. (1996) *J. Magn. Reson., Ser. B 110*, 96−101.
44. Mori, S., van Zijl, P. C., and Shortle, D. (1997) *Proteins 28*, 325−332.
45. Moore, C. D., al-Misky, O. N., and Lecomte, J. T. J. (1991) *Biochemistry 30*, 8357−8365.
46. Johnson, C. E., and Bovey, F. A. (1958) *J. Chem. Phys. 29*, 1012−1014.
47. Kao, Y.-H., and Lecomte, J. T. J. (1993) *J. Am. Chem. Soc. 115*, 9754−9762.
48. Brünger, A. T. (1992) *X-PLOR. Version 3.1. A system for X-ray crystallography and NMR*, Yale University Press, New Haven, CT.
49. Laskowski, R. A., Rullmannn, J. A., MacArthur, M. W., Kaptein, R., and Thornton, J. M. (1996) *J. Biomol. NMR 8*, 477−486.
50. Vriend, G. (1990) *J. Mol. Graphics 8*, 52−56.
51. Lee, B., and Richards, F. M. (1971) *J. Mol. Biol. 55*, 379−400.
52. Hubbard, S. J., and Thornton, J. M. (1993) *NACCESS*, Department of Biochemistry and Molecular Biology, University College London, London.
53. Chothia, C. (1976) *J. Mol. Biol. 105*, 1−12.
54. Creamer, T. P., Srinivasan, R., and Rose, G. D. (1997) *Biochemistry 36*, 2832−2835.
55. Banci, L., Bertini, I., Ferroni, F., and Rosato, A. (1997) *Eur. J. Biochem. 249*, 270−279.
56. Munoz, V., and Serrano, L. (1995) *J. Mol. Biol. 245*, 275−296.
57. Lindestrom-Lang, K. U. (1955) *Chem. Soc. 2*, 1−20.
58. Hvidt, A., and Nielsen, S. O. (1966) *Adv. Protein Chem. 21*, 287−386.
59. Hargrove, M. S., and Olson, J. S. (1996) *Biochemistry 35*, 11310−11318.
60. McLachlan, S. J., La Mar, G. N., and Lee, K.-B. (1988) *Biochim. Biophys. Acta 957*, 430−445.
61. La Mar, G. N., Burns, P. D., Jackson, J. T., Smith, K. M., Langry, K. C., and Strittmatter, P. (1981) *J. Biol. Chem. 256*, 6075−6079.
62. Pochapsky, T. C., Sligar, S. G., McLachlan, S. J., and La Mar, G. N. (1990) *J. Am. Chem. Soc. 112*, 5258−5263.
63. Sarma, S., Dangi, B., Yan, C., DiGate, R. J., Banville, D. L., and Guiles, R. D. (1997) *Biochemistry 36*, 5645−5657.
64. Lee, K. B., La Mar, G. N., Kehres, L. A., Fujinari, E. M., Smith, K. M., Pochapsky, T. C., and Sligar, S. G. (1990) *Biochemistry 29*, 9623−9631.
65. Mortuza, G. B., and Whitford, D. (1997) *FEBS Lett. 412*, 610−614.
66. Aung, H., Bocola, M., Schleper, S., and Rohm, K. (2000) *Biochim. Biophys. Acta 1481*, 349−359.
67. Aimes, R. T., Hemmer, W., and Taylor, S. S. (2000) *Biochemistry 39*, 8325−8332.
68. Greenwald, J., Le, V., Butler, S. L., Bushman, F. D., and Choe, S. (1999) *Biochemistry 38*, 8892−8898.
69. Falzone, C. J., Wright, P. E., and Benkovic, S. J. (1994) *Biochemistry 33*, 439−442.
70. Luque, I., and Freire, E. (2000) *Proteins Suppl. 4*, 63−71.
71. Moore, C. D., and Lecomte, J. T. J. (1990) *Biochemistry 29*, 1984−1989.
72. Moore, C. D. (1993) Ph.D. Dissertation, The Pennsylvania State University, University Park, PA.
73. Eigen, M. (1964) *Angew. Chem., Int. Ed. 3*, 1−19.
74. Anjum, F., Rishi, V., and Ahmad, F. (2000) *Biochim. Biophys. Acta 1476*, 75−84.
75. Wang, A., Robertson, A. D., and Bolen, D. W. (1995) *Biochemistry 34*, 15096−15104.
76. Saunders, A. J., Davis-Searles, P. R., Allen, D. L., Pielak, G. J., and Erie, D. A. (2000) *Biopolymers 53*, 293−307.
77. Qu, Y., Bolen, C. L., and Bolen, D. W. (1998) *Proc. Natl. Acad. Sci. U.S.A. 95*, 9268−9273.
78. Sandström, J. (1982) *Dynamic NMR spectroscopy*, Academic Press, London.
79. Beck von Bodman, S., Schuler, M. A., Jollie, D. R., and Sligar, S. G. (1986) *Proc. Natl. Acad. Sci. U.S.A. 83*, 9443−9447.
80. Sligar, S. G., and Egeberg, K. D. (1987) *J. Am. Chem. Soc. 109*, 7896−7897.
81. Rodriguez, J. C., and Rivera, M. (1998) *Biochemistry 37*, 13082−13090.
82. Ihara, M., Takahashi, S., Ishimori, K., and Morishima, I. (2000) *Biochemistry 39*, 5961−5970.
83. Barrick, D., Ho, N. T., Simplaceanu, V., Dahlquist, F. W., and Ho, C. (1997) *Nat. Struct. Biol. 4*, 78−83.
84. Hargrove, M. S., Barrick, D., and Olson, J. S. (1996) *Biochemistry 35*, 11293−11299.
85. La Mar, G. N., Pande, U., Hauksson, J. B., Pandey, R. K., and Smith, K. M. (1989) *J. Am. Chem. Soc. 111*, 485−491.
86. Lecomte, J. T. J., and Cocco, M. J. (1990) *Biochemistry 29*, 11057−11067.
87. Hunter, C. L., Lloyd, E., Eltis, L. D., Rafferty, S. P., Lee, H., Smith, M., and Mauk, A. G. (1997) *Biochemistry 36*, 1010−1017.
88. Kraulis, P. (1991) *J. Appl. Crystallogr. 24*, 946−950.
89. Bundi, A., and Wüthrich, K. (1979) *Biopolymers 18*, 285−297.
90. Robinson, C. R., Liu, Y., Thomson, J. A., Sturtevant, J. M., and Sligar, S. G. (1997) *Biochemistry 36*, 16141−16146.

BI002681G